A New *I–V* Model for Short Gate-Length MESFET's

Shan-Ping Chin, *Student Member, IEEE*, and Ching-Yuan Wu, *Member, IEEE*

***Abstract*—A new *I–V* model for short gate-length MESFET's operated in the turn-on region is proposed, in which the two-dimensional potential distribution contributed by the depletion-layer charges under the gate and in the ungate region are separately obtained by conventional 1D approximation and Green's function solution technique. Moreover, the bias-dependent parasitic resistances due to the modulation of depletion layer in the ungate region for non-self-alignment MESFET's are also taken into account in the developed *I–V* model. It is shown that good agreements are obtained between the developed new *I–V* model and the results of 2D numerical analysis. Moreover, comparisons between the proposed analytical model and the experimental data are made and excellent agreements are obtained.**

NOMENCLATURE

ϵ	Dielectric permittivity of semiconductor.
q	Elemental charge ($= 1.6 \times 10^{-19}$ C).
b	Active-layer thickness.
L_g	Gate length.
$L_{gd}(L_{gs})$	Spacing between the gate and the drain (source).
V_{bi}	Built-in potential of Schottky-barrier gate.
V_{gs}	Gate–source voltage.
V_{ds}	Drain–source voltage.
$\Psi(x, y)$	Two-dimensional potential distribution.
$\Psi_q(x, y)$	Component of the two-dimensional potential distribution contributed by the depletion charge under the gate.
$\Psi_l(x, y)$	Component of the two-dimensional potential distribution contributed by the depletion charge in the ungate region.
$n(x, y)$	Electron-density distribution.
$N_d(x, y)$	Doping profile.
$\Psi_c(x)$	Potential distribution along the channel ($= \Psi(x, b)$).
$E(x)$	Electric field distribution along the channel ($= -d\Psi_c(x)/dx$).
$v_n(E)$	Drift velocity of electrons.
$R_s(R_d)$	Parasitic series resistance at the source(drain) side.
$k_n(k_m)$	Eigenvalue of the Green's function in the ungate (gate) region ($k_n = n\pi/b$ and $k_m = (m - 1/2)\pi/b$).
I_{ds}	Drain current.
$h(x)$	Depletion-layer thickness in the channel region.
$h_d(h_s)$	Depletion-layer thickness at the drain(source) side of the gate.
$\rho(x, y)$	Charge density distribution.
μ_n	Low-field mobility.
κ_a	Parameter used to describe the effect of the channel field on the low-field mobility.
v_{sl}	Scattering-limited velocity.
E_c	Critical electric field.
B_m	Fourier coefficient for the one-dimensional potential distribution produced by the ionized impurity concentration $\left(= \frac{2}{b}\int_0^b \sin(k_m y)\left[\int_0^y \frac{qN_d(y')}{\epsilon} y'\,dy' + y\int_0^y \frac{qN_d(y')}{\epsilon}\,dy'\right]\right)$.
$N_{d,n}^s(x)$	Fourier coefficient for the doping profile in the ungate region at the source side $\left(= \frac{c}{b}\int_0^b N_d(x, y)\cos(k_n y)\,dy,\ c = 1 \text{ for } n = 0 \text{ and } c = 2 \text{ for } n > 1\right)$.
$N_{d,n}^d(x)$	Fourier coefficient for the doping profile in the ungate region at the drain side $\left(= \frac{c}{b}\int_0^b N_d(x, y)\cos(k_n y)\,dy,\ c = 1 \text{ for } n = 0 \text{ and } c = 2 \text{ for } n > 1\right)$.
$n_{d,m}$	Fourier coefficient for the doping profile under the gate $\left(= \frac{2}{b}\int_0^b N_d(x, y)\sin(k_m y)\,dy\right)$.
V_1	Average one-dimensional potential due to the depletion-layer charges under the gate $\left(= \sum_{m=1}^{\infty} \frac{2B_m}{(2m - 1)\pi}\right)$.

Manuscript received July 16, 1992; revised November 30, 1992. This work was supported by the National Science Council, Taiwan, Republic of China, under Contract NSC-81-0404-E0009-139. The review of this paper was arranged by Associate Editor A. H. Marshak.

The authors are with the Advanced Semiconductor Device Research Laboratory and Institute of Electronics, National Chiao-Tung University, Hsinchu, Taiwan, ROC.

IEEE Log Number 9206971.

0018-9383/93$03.00

T_{mn} Element of the transfer matrix

$$\left(= \frac{2}{b} \int_0^b \sin(k_m y) \cos(k_n y)\, dy \right).$$

I. Introduction

GALLIUM ARSENIDE (GaAs) MESFET has become a very important device for high-speed IC and microwave applications. The MESFET device with a gate-length of quarter-micrometer has been fabricated [1], but the characteristics of the scaled-down devices are shown to be significantly affected by the two-dimensional field distribution, resulting in a strong threshold-voltage shift and finite saturation conductance. These two-dimensional effects have not been properly considered in previously published analytic I–V models [2]–[6]. Recently, an analytical I–V model for the non-self-aligned MESFET device has been proposed [7] by solving the 2D Poisson's equation using a trial-function method. However, this model does not exactly consider the boundary conditions at the free surface and the bias-dependent parasitic source and drain resistances [8], [9]. Moreover, a nonphysical adjusting parameter must be used to correlate the source (drain) parasitic resistance with bias, resulting in large discrepancy between calculated results and experimental data in the knee region. More recently, an analytical model considering the two-dimensional field distribution at the drain side under the gate has been developed [10]. However, this model is not applicable for short-gate-length MESFET devices because the effect of threshold-voltage shift cannot be described by this model.

The primary problem for modeling the turn-on I–V characteristics of a short gate-length MESFET is that the strongly coupled nonlinear partial differential equations must be solved simultaneously, and this makes the development of the analytic model difficult. The purpose of this paper is to develop a 2D analytic model for describing the effect of 2D potential distribution on the I–V characteristics of a MESFET device operated in the turn-on region. Based on the derived 2D potential distribution, a new analytic I–V model for short gate-length MESFET's is developed and compared to the results of 2D numerical analysis. The major features of our model are: 1) the Green's function solution technique for the 2D Poisson's equation is adopted and further simplified to obtain 2D potential distribution contributed by the depletion-layer charges in the ungate region [11]; 2) the potential distribution contributed by the depletion-layer charges under the gate is only part of the 2D potential distribution and can be calculated by conventional 1D approximation [12]; 3) the bias-dependent parasitic source and drain resistances due to the formation of the depletion layer in the ungate region for non-self-aligned MESFET's are considered in the developed I–V model.

In Section II, the basic equations and boundary conditions for different MESFET structures are described. Moreover, a simplified solution based on the Green's function solution technique for the 2D Poisson's equation is proposed. In Section III, a new I–V model is developed, and an iterative method is used to determine the channel potential and the drain current self-consistently. In Section IV, the derived channel potential and I–V characteristics of the developed model are compared with those calculated by 2D numerical analysis and conventional Gradual-Channel Approximation (GCA) [12]. Moreover, the effects of the bias-dependent parasitic resistances on the I–V characteristics of MESFET's are also discussed in this section. Finally, conclusions are given in Section V.

II. A Simplified Analytical Model for the 2D Potential Distribution

The threshold voltage is one of the key design parameters for a MESFET device. It is known that the threshold voltage of a short gate-length MESFET is different from that of a long gate-length device due to the 2D effects. However, the mathematical treatments of the 2D partial differential equations such as the Poisson's equation and the current continuity equations are complicated and make the development of a simple analytical model difficult. Therefore, the understanding of the 2D effects is very important for developing a simple analytical model. In this section, an analytical solution of the 2D Poisson's equation based on the Green's function solution technique [11] and the conventional 1D approximation [12] is developed for a MESFET operated in the turn-on region.

The cross-sectional views for both non-self-aligned MESFET and self-aligned MESFET devices operated in the turn-on region are shown in Fig. 1(a) and (b), respectively, where the x-coordinate represents the direction along the surface and the y-coordinate represents the direction perpendicular to the surface. From the 2D analysis using the Green's function solution technique [11] and the boundary conditions shown in Fig. 1(a), the 2D potential under the gate can be expressed by

$$\Psi(x, y) = \Psi_q(x, y) + \Psi_l(x, y) \tag{1}$$

where $\Psi_q(x, y)$ is the component of the potential distribution contributed by the depletion-layer charges under the gate and $\Psi_l(x, y)$ is the component of the potential distribution contributed by the depletion-layer charges in the ungate region.

Following the conventional analysis, $\Psi_q(x, y)$ can be calculated by the conventional 1D approximation

$$\Psi_q(x, y) = \int_0^y \frac{qN_d(x, y')}{\epsilon} y'\, dy' + y \int_y^{h(x)} \frac{qN_d(x, y')}{\epsilon}\, dy' - V_{gs} + V_{bi}. \tag{2}$$

It should be noted that the approximation in (2) is based on the fact that the depletion-layer thickness under the gate $h(x)$ is a slowly varying function along the channel. The channel potential is obtained by setting the integra-

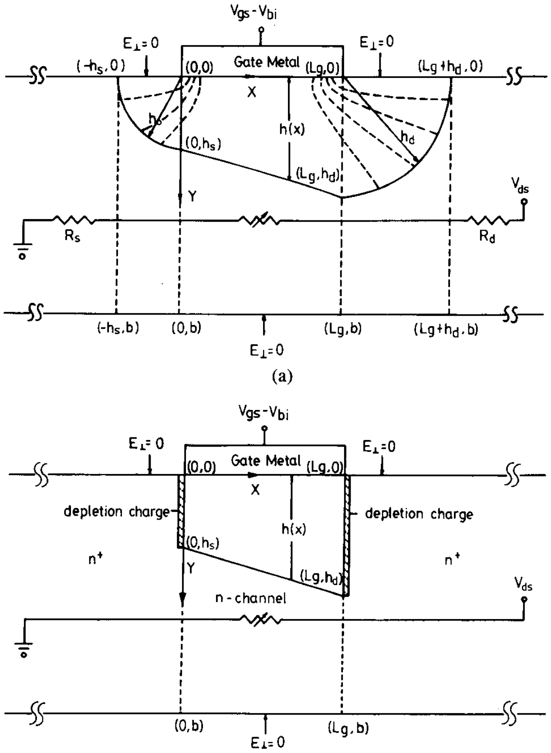

(a)

(b)

Fig. 1. The schematic diagram of a MESFET operated in the turn-on region for developing the 2D analytical solution and showing the penetration of the sidewall electric field into the gate-controlled region: (a) the non-self-aligned structure and (b) the self-aligned structure.

tion limit with $y = h(x)$ in (2), i.e.,

$$\begin{aligned}\Psi_c(x) &= \Psi_q(x, h(x)) \\ &= \int_0^{h(x)} \frac{qN_d(x, y')}{\epsilon} y' \, dy' - V_{gs} + V_{bi}. \qquad (3)\end{aligned}$$

Based on the Green's function technique [11], $\Psi_l(x, y)$ can be expressed by

$$\Psi_l(x, y) = \sum_m \left[\left(A_m^s \frac{\sinh k_m(L_g - x)}{\sinh (k_m L_g)} + A_m^d \frac{\sinh (k_m x)}{\sinh (k_m L_g)}\right] \sin (k_m y) \qquad (4)$$

where

$$A_m^s = \frac{2}{b} \int_0^b [\Psi(0, y) - \Psi_q(0, y)] \sin (k_m y) \, dy$$

and

$$A_m^d = \frac{2}{b} \int_0^b [\Psi(L_g, y) - \Psi_q(L_g, y)] \sin (k_m y) \, dy$$

are the Fourier coefficient for the excess sidewall potential at the source and drain sides of the gate, respectively. Note that $\Psi_l(x, y)$ almost decays exponentially due to the termination of the electrical flux by the gate metal, as shown in Fig. 1. This component of the potential distribution is very important for modeling the saturation behavior and the short gate-length effect of a MESFET.

From the numerical analysis, it is known that the first term of Fourier series in (4) is a dominant term for describing $\Psi_l(x, y)$ at the gate edge because the higher order terms of $\Psi_l(x, y)$ decay rapidly. Therefore, (4) can be approximated by keeping only the first term

$$\Psi_l(x, y) \cong \left[\left(A_1^s \frac{\sinh k_l(L_g - x)}{\sinh (k_l L_g)} + A_1^d \frac{\sinh (k_1 x)}{\sinh (k_1 L_g)}\right] \sin (k_1 y). \qquad (5)$$

As a result, the accurate channel potential can be obtained from (3)–(5), and is expressed by

$$\Psi_c(x) = \int_0^{h(x)} \frac{qN_d(x, y')}{\epsilon} y' \, dy' + A_1^s \frac{\sinh k_1(L_g - x)}{\sinh (k_1 L_g)} + A_1^d \frac{\sinh (k_1 x)}{\sinh (k_1 L_g)} - V_{gs} + V_{bi} \qquad (6)$$

where A_1^s and A_1^d in (6) must be predetermined before calculating the two-dimensional potential distribution for a given $h(x)$. These coefficients are mainly due to the 2D effects induced by the depletion-layer charges in the ungate region. Thus the values of A_1^s and A_1^d depend on the source/drain structure. According to different source/drain structures, the calculations of A_1^s and A_1^d for both self-aligned and non-self-aligned structures can be obtained.

Since the lateral electrical flux is completely terminated by the n$^+$-region for a self-aligned structure and the electrical field in the n$^+$-region is negligible, thus the potential distribution at the source (drain) side can be written as $\Psi(x, 0) = 0$ and $\Psi(x, L_g) = V_{ds}$. Substituting the above boundary conditions into (6) and performing the Fourier transformation, A_1^d and A_1^s for a self-aligned MESFET operated in the subthreshold region can be expressed as

$$A_1^{s(d)} = F_1^a\left(\frac{\Delta V_s(d)}{V_p}\right) = \frac{4}{\pi} \Delta V_{s(d)} - B_1 \qquad (7)$$

where the superscript a is used to denote the self-aligned structure and $B_1 \cong 1.03 V_p$ for uniform doping profile.

The linear dependence of $A_1^{s(d)}$ for a self-aligned MESFET on the voltage drops can be found in (7). However, the complexity for modeling $A_1^{s(d)}$ of a non-self-aligned MESFET is raised by the boundary conditions in the ungate region. A simplified technique based on the Green's function solution technique has been developed [11] to calculate A_1^s and A_1^d when the device is operated in the subthreshold region. Based on this method, A_1^s and A_1^d can be written as

$$A_1^s = V_p\left[a_1 + b_1\left(\frac{V_{bi} - V_{gs} - V_1}{V_p} - c_1\right)^{1/2}\right] \qquad (8)$$

$$A_1^d = V_p \left[a_2 + b_1 \left(\frac{V_{ds} + V_{bi} - V_{gs} - V_1}{V_p} - c_2 \right)^{1/2} \right] \tag{9}$$

where

$$a_1 = [\beta A_1^d + \eta]/(\alpha V_p) - 64/(\pi^3 \alpha^2)$$

$$b_1 = 8/(\pi\alpha)$$

$$c_1 = 2a_1/\pi - 64/(\pi^4 \alpha^2)$$

$$a_2 = [\beta A_1^s + \eta]/(\alpha V_p) - 64/(\pi^3 \alpha^2)$$

and

$$c_2 = 2a_2/\pi - 64/(\pi^4 \alpha^2).$$

Note that α, β, V_1, and V_p are the structure parameters, which are independent of bias conditions and are expressed as

$$\alpha = \frac{\pi}{2} \coth (k_1 L_g) + \frac{1.4}{\pi} \tag{10a}$$

$$\beta = \frac{\pi}{2} \frac{1}{\sinh (k_1 L_g)} \tag{10b}$$

$$V_1 = \sum_{m=1}^{\infty} \frac{2B_m}{(2m-1)\pi} \tag{10c}$$

$$V_p = \frac{q N_{d,0}^s}{2\epsilon} b^2 \tag{10d}$$

and

$$\eta = b \sum_{n=1}^{\infty} T_{1n} \left(\sum_{m1=1}^{\infty} k_n B_{m1} T_{m1,n} - \frac{q N_{d,n}^s}{k_n \epsilon} \right). \tag{10e}$$

The above coefficients are used to model the effects of nonuniform doping profile. For the uniform profile case, these coefficients can be derived as: $a_1 = -0.77$, $b_1 = 1.26$, $c_1 = 0.33$, and $V_1 = 0.67 V_p$.

Further simplification with $a_1 = a_2$ can be made by assuming $1/\sinh (k_1 L_g) \cong 0$. As a result, (8) and (9) can be rewritten as

$$A_1^{s(d)} = F_1^n \left(\frac{\Delta V_{s(d)}}{V_p} \right)$$

$$= V_p \left[a_1 + b_1 \left(\frac{\Delta V_{s(d)} - V_1}{V_p} - c_1 \right)^{1/2} \right] \tag{11}$$

where the superscript n is used to denote the non-self-aligned structure; $\Delta V_s = V_{bi} - V_{gs} + I_{ds} R_s$ and $\Delta V_d = V_{bi} - V_{gs} + V_{ds} - I_{ds}(R_s + R_d)$ are the potential drops across the depletion layers between the gate and the source and the drain, respectively.

It should be noted that the calculations of these coefficients become complicated because the mobile carriers will contribute to $\Psi_I(x, y)$ when the device is operated in the turn-on region. Checking the results of 2D numerical analysis is very important for making a proper assumption. The dependence of these coefficients on bias conditions can be extracted from the results of numerical analysis by the following expression derived from (1):

$$A_1^d = \frac{2}{b} \int_0^b \sin (k_1 y') \, [\Psi(L_g, y') - \Psi_q(L_g, y')] \, dy' \tag{12}$$

where $\Psi(x, y)$ and $\Psi_q(x, y)$ are obtained from the results of 2D numerical analysis. It is noted that the lateral electric field at both sides of the gate is originally induced by the depletion-layer charges between the gate and the source (drain). The magnitude of $A_1^{s(d)}$ can be reasonably expressed as a function of the voltage drop between the gate and the source (drain) side of the depletion layer $\Delta V_s(\Delta V_d)$. The numerical results of (12) versus the voltage drop across the depletion layer between the gate and the drain are indicated by the solid line in Fig. 2. The discrepancy of A_1^d between the device operated in the saturation region and that operated in the subthreshold region is mainly due to the component of the potential distribution contributed by the mobile carriers. However, it is interesting to note that this discrepancy is not obvious due to the fact that the mobile carriers in the high-field (high-velocity) region are small in order to keep a constant channel current. Since the contribution from the mobile carriers to the Fourier coefficients at the sidewall is not important, the mobile carriers can be neglected in the calculation when the device is operated in the saturation region. Another feature, which can be obtained from Fig. 2, is that the A_1^d profile versus the voltage drop becomes linear for a small voltage drop. Based on these results, we can avoid the complex mathematical treatment by making a proper approximation for the characteristics of the $A_1^s(A_1^d)$ profile as follows:

$$A_1^{s(d)} = F_1^{n(a)} \left(\frac{\Delta V_{s(d)}}{V_p} \right) S \left(\frac{\Delta V_{s(d)}}{V_p} - 1.3 \right) + F_2^{n(a)} \left(\frac{\Delta V_{s(d)}}{V_p} \right) S \left(1.3 - \frac{\Delta V_{s(d)}}{V_p} \right) \tag{13}$$

where $F_1^n(x)$ and $F_1^a(x)$ are the functions expressed in (7) and (9), respectively; $F_2^n(x)$ and $F_2^a(x)$ are the linear functions used to characterize A_1^d in low-voltage drop for both non-self-aligned and self-aligned MESFET's. $F_2^{n(a)}(x)$ can be written as

$$F_2^{n(a)} \left(\frac{\Delta V_{s(d)}}{V_p} \right) = \theta^{n(a)} \frac{\Delta V_{s(d)}}{V_p} \tag{14}$$

where $\theta^{n(a)} = F_1^{n(a)}(1.3)/1.3$; $S(x)$ is a smooth function to connect $F_1^{n(a)}$ and $F_2^{n(a)}$ in a smooth manner and can be written as

$$S(x) = (\tanh (x/0.1) + 1)/2. \tag{15}$$

The results of (13) are shown in Fig. 2(a) and (b) as indicated by the broken lines with an asterisk for non-self-aligned and self-aligned MESFET's, respectively. It is clearly seen that the results are acceptable from the viewpoint of simplifying the mathematical treatment.

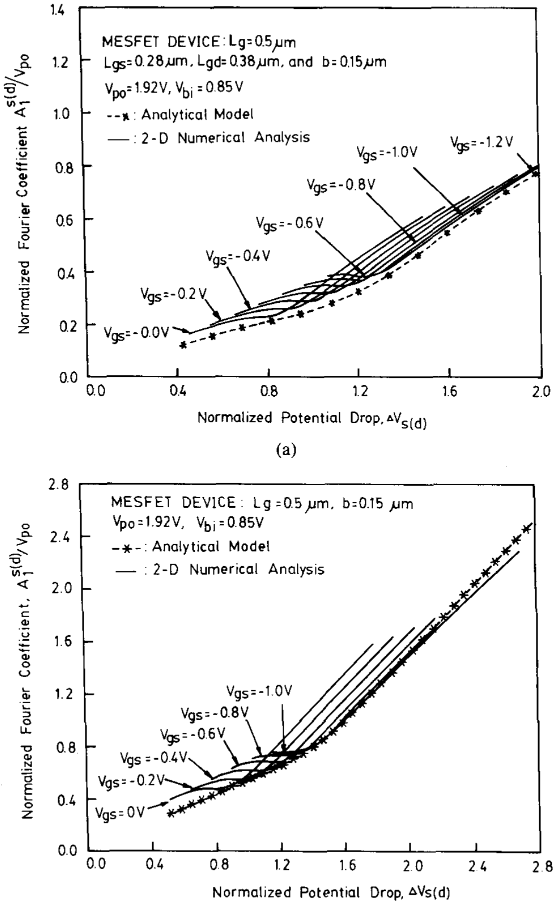

(a)

(b)

Fig. 2. The normalized $A_1^d(A_1^s)$ profile as a function of the normalized voltage drop for (a) the non-self-aligned structure and (b) the self-aligned structure. The solid lines are extracted from the results of 2D numerical analysis for various V_{gs}, and the broken lines with asterisks indicate analytical approximation.

III. The *I–V* Model

It is noted that the electron-density distribution $n(x, y)$ must be self-consistently calculated by including 2D current continuity equations. In general, the self-consistent calculation can only be obtained by using numerical analysis. In order to obtain an analytical solution, some reasonable approximations are made. The first approximation is that the current flow in the y-direction can be neglected, which is valid for modern devices with channel thickness smaller than the channel length. The second approximation is that the variation of electron mobility versus the y-position can be neglected for simplicity. The other approximations used are the abrupt depletion edge and the quasi-neutral condition in the channel region. Based on these approximations, the drain current can be expressed as

$$I_{ds} = qWv_n(E) \int_{h(x)}^{b} N_d(x, y)\, dy \tag{16}$$

where

$$v_n(E) = \mu_n(E) \frac{d\Psi_c(x)}{dx}. \tag{17}$$

It is well known that the accurate I–V model is strongly dependent on the mobility model. The choice of a suitable form for the mobility is not only important for an accurate description of physical phenomena in short gate-length MESFET's but also necessary for simplifying the mathematical treatment. In general, the electric field perpendicular to the current flow is very weak for a MESFET device operated in the turn-on region and, therefore, the dependence of carrier mobility on the perpendicular electric field can be neglected. The mobility model used in our developed I–V model is expressed by

$$\mu_n(E) = \mu_n - \kappa_a E, \qquad \text{for } E < E_c \tag{18a}$$

$$= \frac{v_a}{E} + \frac{\mu_b(1 - E_c/E)}{1 + \mu_b(E - E_c)/(v_{sl} - v_a)}, \qquad \text{for } E > E_c. \tag{18b}$$

Note that the carrier mobility expressed in low field and high field are described by (18a) and (18b), respectively. The parameters v_a and κ_a can be eliminated by equating (18a) and (18b) and the differentiations of (18a) and (18b) with respect to E at $E = E_c$. The results can be expressed by

$$v_a = \frac{(\mu_n + \mu_b)E_c}{2} \tag{19}$$

and

$$\kappa_a = \frac{\mu_n E_c - v_a}{E_c^2}. \tag{20}$$

It is clearly seen that the proposed mobility model gives a smooth and continuous curve for the drift velocity versus the channel field. The drain current I_{ds} can be obtained from (16) if the doping concentration is uniform

$$I_{ds} = qWv_n(E)N_d(b - h(x)). \tag{21}$$

Rearranging (21), the following equation can be obtained:

$$v_n(E) = \frac{I_{ds}}{qWN_d(b - h(x))} \tag{22}$$

where $h(x)$ can be calculated from (6) in terms of $\Psi_c(x)$

$$h(x) = \left[\frac{2\epsilon}{qN_d}\left(\Psi_c(x) - V_{bi} + V_{gs} - A_1^s \frac{\sinh k_1(L_g - x)}{\sinh (k_1 L_g)} - A_1^d \frac{\sinh (k_1 x)}{\sinh (k_1 L_g)}\right)\right]^{1/2}, \qquad \text{for } 0 \le x \le L_g. \tag{23}$$

It should be noted that the depletion-layer thickness in the ungate region is bias-dependent for a non-self-aligned MESFET. The bias-dependent parasitic source and drain resistance due to the formation of the depletion layer in the ungate region can be calculated by assuming the cylindrical shape as shown in Fig. 1(a) and can be expressed as

$$h(x) = (h_s^2 - x^2)^{1/2}, \qquad \text{for } -h_s < x < 0, \tag{24a}$$

$$h(x) = [h_d^2 - (x - L_g)^2]^{1/2}, \qquad \text{for } L_g < x < L_g + h_d. \tag{24b}$$

Using (17) and (22), $d\Psi_c(x)/dx$ can be expressed by

$$\frac{d\Psi_c(x)}{dx} = f\left(\frac{I_{ds}}{qWN_d(b - h(x))}\right) \tag{25}$$

where $f(v_n)$ can be expressed as

$$\begin{aligned} \frac{d\Psi_c(x)}{dx} = f(v_n) &= \frac{\mu_n - (\mu_n^2 - 4\kappa_a v_n)^{1/2}}{2\kappa_a}, \\ &\qquad \text{for } v_n < v_a \\ &= E_c + 1/[\mu_b/(v_n - v_a) - \mu_b/(v_{sl} - v_a)], \\ &\qquad \text{for } v_a \leq v_n < v_{sl} \\ &= \infty, \qquad \text{for } v_n \geq v_{sl}. \end{aligned} \tag{26}$$

Note that although the mobility model expressed in (18) is used to describe the electron behavior in the semiconductor, other types of the mobility model can be also treated by (25) provided that the inverse function of the mobility can be calculated.

$\Psi_c(x)$ can be obtained by performing the integration of (25)

$$\Psi_c(x) = I_{ds}R_s + \int_{-h_s}^{x} f\left(\frac{I_{ds}}{qWN_d(b - h(x))}\right) dx \tag{27}$$

and I_{ds} must be determined by matching to the bias condition iteratively, i.e.,

$$V_{ds} - I_{ds}(R_s + R_d) = \int_{-h_s}^{L_g + h_d} f\left(\frac{I_{ds}}{qWN_d(b - h(x))}\right) dx. \tag{28}$$

The series resistances (R_s and R_d) used in (27) and (28) are calculated from the structure of the MESFET device. For a non-self-aligned MESFET, R_s and R_d can be expressed as

$$R_s = \frac{L_{gs}}{qN_d\mu_n W} \tag{29}$$

and

$$R_d = \frac{L_{gd}}{qN_d\mu_n W}. \tag{30}$$

For a self-aligned MESFET, R_s and R_d are negligibly small due to the heavy doping in the source and drain regions. The drain current for the device operated in the saturation region can be calculated by (26) and the channel field will become infinite when the electron drift velocity reaches v_{sl}. The determination of the saturation current is the same as the condition of channel pinch-off used in the conventional I-V model.

IV. RESULTS AND DISCUSSIONS

In order to demonstrate the validity of the proposed new model, a 2D device simulator [13] based on the conventional semiconductor device equations is used to verify the accuracy of the developed model in this section. Comparisons of the channel potential among the results of numerical analysis, conventional 1D approach, and proposed new model (6) for different gate lengths are shown in Fig. 3, where the charge density distribution $\rho(x, y)$ used in these calculations are obtained from the results of 2D numerical analysis. It is clearly seen that large discrepancy between conventional 1D approach and 2D numerical analysis is mainly due to the penetration of the lateral field contributed by the depletion-layer charges in the ungate region. However, satisfactory agreements between the 2D numerical analysis and the new model are obtained because the lateral field due to the depletion-layer charges at both sides of the ungate region as expressed in (6) has been considered. It is clearly shown that the channel potential calculated by (6) is valid for the gate length down to quarter-micrometer range.

In order to show the validity of the proposed analytical I-V model, comparisons between the developed analytical I-V model and the 2D numerical analysis are made for a non-self-aligned structure and are shown in Fig. 4 for the gate lengths varied from 1.0 to 0.3 μm. It is clearly seen that good agreements are obtained even for the gate length down to 0.3 μm. Note that the device parameters including those in the mobility model are known in the 2D numerical analysis, therefore no fitting or adjusting parameters are used to compare the results between the proposed new model and the 2D numerical analysis. The slight discrepancy for 0.3-μm gate-length device is mainly caused by overlooking the potential distribution contributed by the mobile carriers in the saturation region. However, the discrepancy is not obvious for the calculated I-V characteristics even for a MESFET with a gate length in the quarter-micrometer range.

Comparisons between the proposed analytical I-V model and the experimental data for a non-self-aligned GaAs MESFET with gate lengths of 1.0 and 0.5 μm are shown in Fig. 5(a) and (b), respectively, and the parameters used in the proposed analytical model are shown in Table I. Note that the parameters used in Table I, except the gate length, are obtained by a curve-fitting optimizer. It is clearly seen that good agreements between the proposed analytical model and the experimental I-V characteristics are obtained. It is quite interesting to argue the

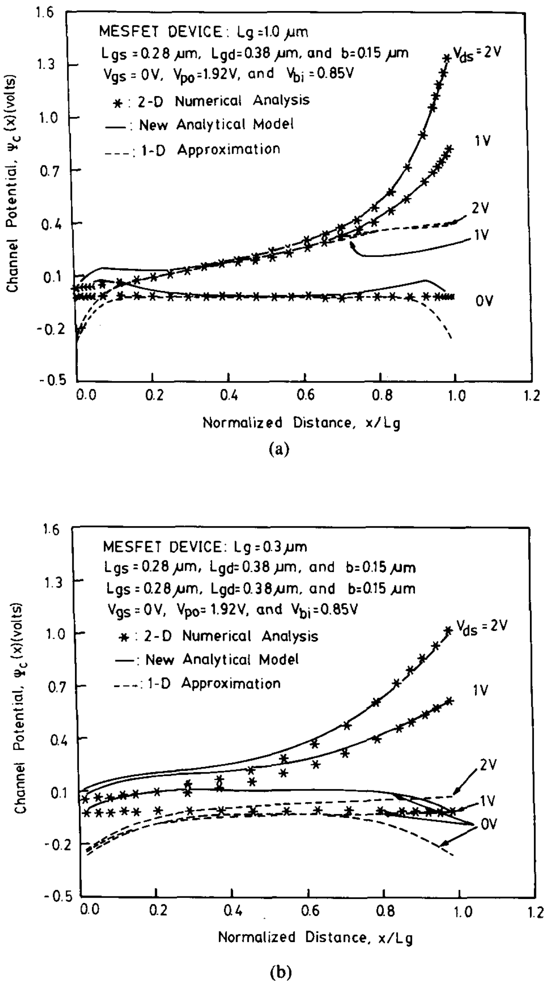

Fig. 3. Comparisons of the channel potential versus the normalized distance (x/L_g) for a non-self-aligned MESFET under various drain biases among the 2D numerical analysis, the 1D approximation, and the 2D analytical model: (a) L_g = 1.0 μm, and (b) L_g = 0.3 μm.

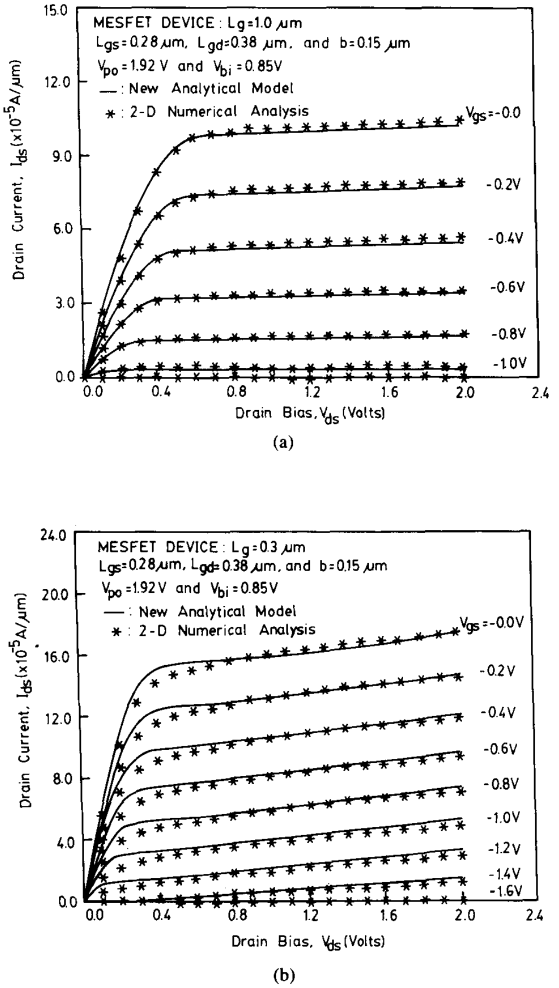

Fig. 4. Comparisons of the I–V characteristics of a non-self-aligned MESFET between the proposed analytical model and the 2D numerical analysis for (a) L_g = 1.0 μm, and (b) L_g = 0.3 μm.

validity of our proposed mobility model for practical GaAs MESFET devices. From our experimental MESFET devices, the effect of differential negative mobility observed from GaAs crystal does not occur. The major reason is that the series parasitic resistance due to the ungate region and the channel of a non-self-aligned structure may smear out the effects of the high drift velocity part of the mobility model with the differential negative mobility characteristic. Therefore, the proposed mobility model can very well simulate the I–V characteristics of practical short-channel GaAs MESFET devices.

Comparisons between the proposed analytical I–V model and the 2D numerical simulation for a self-aligned MESFET with 0.5-μm gate length are shown in Fig. 6, in which it is shown that the 2D effects in a self-aligned MESFET are much stronger than those in a non-self-aligned MESFET. It is clearly seen that good agreements between the proposed analytical I–V model and the 2D numerical analysis are also obtained for a self-aligned structure. Comparisons between the proposed new I–V model and the model calculated by using the conventional Gradual-Channel Approximation (GCA) [12] for a 1.0-μm gate-length device are shown in Fig. 7. It is clearly seen that the difference becomes very large when the device is operated in the saturation region. This implies that the saturation behavior of a MESFET device is strongly affected by the 2D potential distribution.

In order to demonstrate the effects of Bias-Dependent Parasitic Resistance (BDPR) due to the formation of the depletion layer between the gate and the source (drain) on the I–V characteristics of non-self-aligned MESFET's, the results with and without BDPR are compared for 0.5-μm gate-length devices, as shown in Fig. 8. It is clearly shown that the effects of the BDPR cannot be neglected for a non-self-aligned MESFET.

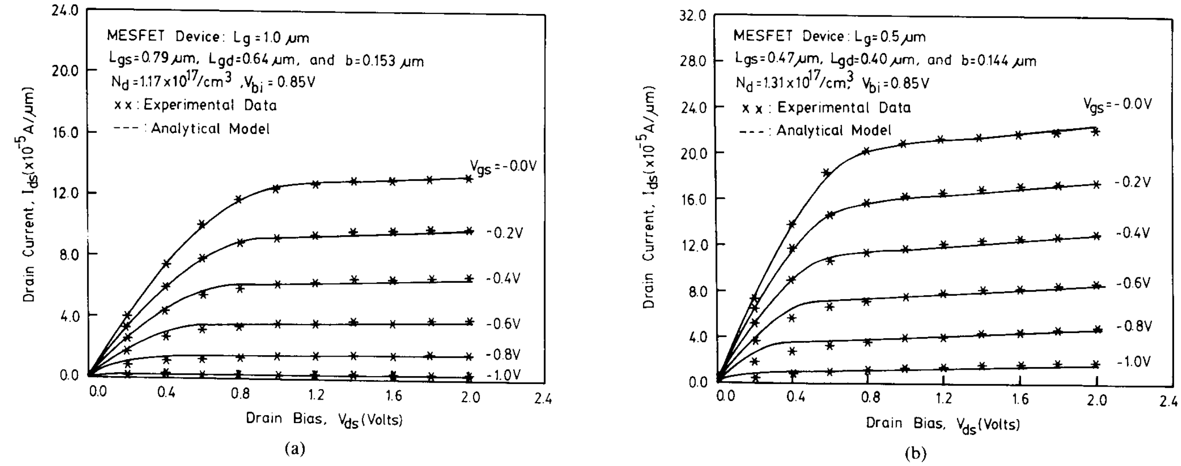

(a)

(b)

Fig. 5. Comparisons of the I-V characteristics of a non-self-aligned MESFET between the proposed analytical model and the experimental I-V characteristics for (a) $L_g = 1.0\ \mu$m and (b) $L_g = 0.5\ \mu$m.

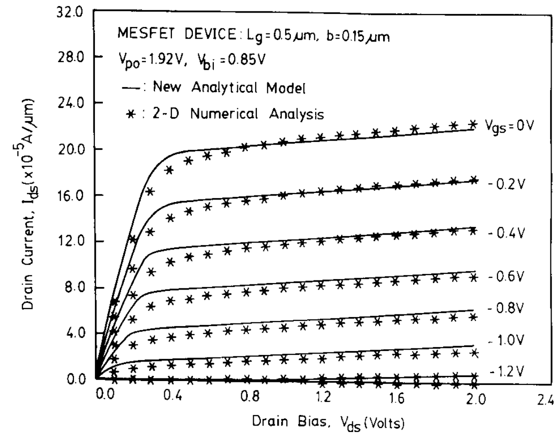

Fig. 6. Comparisons of the I-V characteristics of a self-aligned MESFET with $L_g = 0.5\ \mu$m between the proposed analytical model and the 2D numerical analysis.

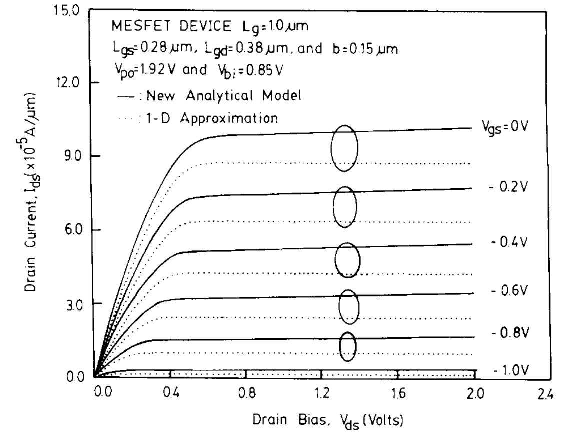

Fig. 7. Comparisons of the I-V characteristics of a non-self-aligned MESFET with $L_g = 1.0\ \mu$m between the proposed analytical model and the results of the 1D approximation.

Table I
The Parameters for Calculating the Drain Current of the Experimental Device

Parameter	Value Device 1	 Device 2
$L_g\,(\mu\text{m})$	1.0	0.5
$\mu_n\,(\text{cm}^2/\text{s/V})$	3435	3483
$v_a\,(\times 10^7\ \text{cm/s})$	2.15	1.80
$\mu_b\,(\text{cm}^2/\text{s/V})$	2760	3000
$v_{sl}\,(\times 10^7\ \text{cm/s})$	4.47	4.90
$N_d\,(\times 10^{17}\ \text{cm}^3)$	1.17	1.31
$b\,(\text{Å})$	1530	1435
$L_{gs}\,(\mu\text{m})$	0.79	0.47
$L_{gd}\,(\mu\text{m})$	0.64	0.40

V. Conclusions

A new two-dimensional (2D) analytical model is developed to calculate the I-V characteristics of short gate-length MESFET's. It is shown that the major drawback

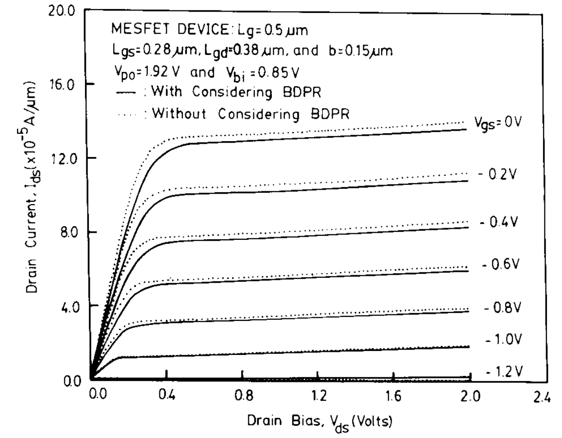

Fig. 8. Comparisons of the I-V characteristics of a non-self-aligned MESFET with $L_g = 0.5\ \mu$m for the proposed analytical model with and without considering the bias-dependent parasitic resistances.

of the conventional 1D approximation is that the penetration of the lateral electric field contributed by the depletion-layer charges in the ungate region is overlooked for both non-self-aligned and self-aligned MESFET's. This lateral electric field is shown to play an important role on the short gate-length effects of a MESFET. In order to accurately model the *I–V* characteristics of a short gate-length MESFET, the effect of the penetration of the lateral field from both sides of the gate is considered in the proposed 2D analytical model by using a simplifying 2D analysis based on the Green's function solution technique. Furthermore, the bias-dependent parasitic source and drain resistances are also taken into account in the proposed *I–V* model for a non-self-aligned MESFET. From comparisons between the proposed analytical model and the 2D numerical analysis, it is shown that the *I–V* characteristics of short gate-length MESFET's can be well predicted by the proposed model. Moreover, from comparisons between the proposed analytical model and the experimental *I–V* characteristics, it is shown that the proposed mobility model is valid for practical GaAs MESFET devices.

References

[1] P. C. Chao, P. M. Smith, S. Wanuga, W. H. Perkins, and E. D. Wolf, "Channel length effects in quarter micrometer gate-length GaAs MESFET's," *IEEE Electron Device Lett.*, vol. EDL-8, pp. 440–442, 1987.

[2] T. Hariu, K. Takahashi and Y. Shibata, "New modeling of GaAs MESFET's," *IEEE Trans. Electron Devices*, vol. ED-30, no. 12, pp. 1743–1749, 1983.

[3] Y. H. Byun, M. S. Shur, A. Peczalski, and F. Schurmeyer, "Gate-voltage dependence of source and drain series resistance and effective gate length in GaAs MESFET's," *IEEE Trans. Electron Devices*, vol. 35, no. 8, pp. 1241–1246, 1988.

[4] M. S. Shur, "Analytical models of GaAs MESFET's," *IEEE Trans. Electron Devices*, vol. ED-25, no. 6, pp. 612–618, 1978.

[5] T. H. Chen and M. S. Shur, "Analytical model of ion-implanted GaAs MESFET's," *IEEE Trans. Electron Devices*, vol. ED-32, no. 1, pp. 18–28, 1985.

[6] P. Pouvil, J. Gautier, and D. Pasquet, "A new analytical model for the GaAs MESFET in the saturation region," *IEEE Trans. Electron Devices*, vol. 35, no. 8, pp. 1215–1222, 1988.

[7] A. Peczalski, C.-H. Chen, M. Shur, and S. M. Baier, "Modeling and characterization of ion-implanted GaAs MESFET's," *IEEE Trans. Electron Devices*, vol. ED-34, no. 4, pp. 726–732, 1987.

[8] S. N. Mohammad, M. B. Patil, J.-I. Chyi, G. B. Gao, and H. Morkoç, "Analytical model for *I–V* characteristics of ion-implanted MESFET's with heavily doped channel," *IEEE Trans. Electron Devices*, vol. 37, no. 1, pp. 11–20, 1990.

[9] C. S. Chang and D.-Y. S. Day, "Analytical theory for current-voltage characteristic and field distribution of GaAs MESFET's," *IEEE Trans. Electron Devices*, vol. 36, no. 2, pp. 269–280, 1989.

[10] C.-H. Chen and D. K. Arch, "The influence of electric field and mobility profile on GaAs MESFET characteristics," *IEEE Trans. Electron Devices*, vol. 36, no. 11, pp. 2405–2416, 1989.

[11] S.-P. Chin and C.-Y. Wu, "A new two-dimensional model for the potential distribution of short gate-length MESFET's and its applications," *IEEE Trans. Electron Devices*, vol. 39, no. 8, pp. 1928–1937, 1992.

[12] W. Shockley, "A unipolar field effect transister," *Proc IRE*, vol. 40, pp. 1365–1376, 1952.

[13] S.-P. Chin and C.-Y. Wu, "A new methodology for two-dimensional numerical simulation of semiconductor devices," *IEEE Trans. Computer-Aided Des.*, vol. 11, no. 12, pp. 1508–1521, Dec. 1992.

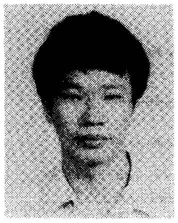

Shan-Ping Chin (S'86) was born in Taiwan, Republic of China, on September 21, 1961. He received the B. S. degree from the Department of Physics, National Tsing-Hua University, Taiwan, Republic of China, in 1985, and the Ph.D. degree from the Institute of Electronics, National Chiao-Tung University, in 1992.

In 1992, he entered the Electronics Research and Service Organization of the Industrial Technology Research Institute. His research activities have been in the device modeling of the deep-submicrometer MESFET's. His present research interests focus on the semiconductor device and the integrated circuit process simulation for VLSI.

Ching-Yuan Wu (M'72) was born in Taiwan, Republic of China, on March 18, 1946. He received the B.S. degree from the Department of Electrical Engineering, National Taiwan University, Taiwan, Republic of China, in 1968, and the M.S. and Ph.D. degrees from the State University of New York (SUNY) at Stony Brook, in 1970 and 1972, respectively.

During the 1972–1973 academic year, he served as a Lecturer at the Department of Electrical Sciences, SUNY, Stony Brook. During the 1973–1975 academic years, he was a Visiting Associate Professor at National Chiao-Tung University (NCTU), Taiwan, Republic of China. In 1976, he became a Full Professor in the Department of Electronics and the Institute of Electronics, NCTU. At NCTU, he had been the Director of Engineering Laboratories and Semiconductor Research Center, during 1974–1980; the Director of the Institute of Electronics, during 1978–1984; and the Dean, College of Engineering, during 1984–1990. He was a principal investigator of the National Electronics Mass Plan—Semiconductor Devices and Integrated-Circuit Technologies during 1976–1979, and had been a Coordinator of the National Microelectronics Researches and High-Level Man-Power Education Committee, National Science Council, Republic of China, during 1982–1988. He has been a Research Consultant at the Electronics Research and Service Organization (ERSO), ITRI; a member of the Academic Review Committee, the Ministry of Education; and the chairman of the Technical Review Committee on Information and Micro-electronics Technologies, the Ministry of Economic Affairs. His research activities have been in semiconductor device physics and modelings, integrated-circuit designs, and technologies. His present research areas focus on the developments of efficient 2D and 3D simulators for deep-submicrometer semiconductor devices, design rules and optimization techniques for deep-submicrometer CMOS devices, and key technologies for deep-submicrometer CMOS devices. He has published over 150 papers in the semiconductor field and has served as a reviewer for international journals such as IEEE Electron Device Letters, IEEE Transactions on Electron Devices, *Solid-State Electronics*, etc. He received the Academic Research Award in Engineering from the Ministry of Education (MOE), in 1979; the outstanding Scholar award from the Chinese Educational and Cultural Foundation, in 1985. He has also received the outstanding research Professor fellowship from the Ministry of Education and the National Science Council (NSC), Republic of China, during 1982–1991.

Dr. Wu is a member of the Honorary Editorial Advisory Board of *Solid-State Electronics* and is a board member of the Chinese Engineering Society.